ISSCR

YAP1 regulates the self-organized fate patterning of hESC-derived gastruloids

Eleonora Stronati,[1,5] Servando Giraldez,[2,4,5] Ling Huang,[3] Elizabeth Abraham,[1] Gillian R. McGuire,[1] Hui-Ting Hsu,[2] Kathy A. Jones,[2] and Conchi Estarás[1,*]

[1]Department of Cardiovascular Sciences, Center for Translational Medicine, Temple University Lewis Katz School of Medicine, Philadelphia, PA, USA
[2]Regulatory Biology Laboratory, The Salk Institute for Biological Studies, 10010 N. Torrey Pines Road, La Jolla, CA 92037, USA
[3]Razavi Newman Integrative Genomics and Bioinformatics Core, The Salk Institute for Biological Studies, La Jolla, CA 92037, USA
[4]Molecular and Cell Biology Laboratory, The Salk Institute for Biological Studies, 10010 N. Torrey Pines Road, La Jolla, CA 92037, USA
[5]These authors contributed equally
*Correspondence: conchi.estaras@temple.edu
https://doi.org/10.1016/j.stemcr.2021.12.012

SUMMARY

The gastrulation process relies on complex interactions between developmental signaling pathways that are not completely understood. Here, we interrogated the contribution of the Hippo signaling effector YAP1 to the formation of the three germ layers by analyzing human embryonic stem cell (hESC)-derived 2D-micropatterned gastruloids. YAP1 knockout gastruloids display a reduced ectoderm layer and enlarged mesoderm and endoderm layers compared with wild type. Furthermore, our epigenome and transcriptome analysis revealed that YAP1 attenuates Nodal signaling by directly repressing the chromatin accessibility and transcription of key genes in the Nodal pathway, including the *NODAL* and *FOXH1* genes. Hence, in the absence of YAP1, hyperactive Nodal signaling retains SMAD2/3 in the nuclei, impeding ectoderm differentiation of hESCs. Thus, our work revealed that YAP1 is a master regulator of Nodal signaling, essential for instructing germ layer fate patterning in human gastruloids.

INTRODUCTION

Gastrulation is a crucial developmental stage when the pluripotent epiblast subsequently converts into the three embryonic germinal layers: mesoderm, ectoderm, and endoderm (Arnold and Robertson, 2009). The success of gastrulation relies largely on the spatiotemporal regulation of the Nodal signaling pathway mediated by extraembryonic signals (Arnold and Robertson, 2009; Meno et al., 1999; Perea-Gomez et al., 2002). Hence, high Nodal activity in the posterior epiblast specifies the primitive streak (PS) (Brennan et al., 2001, 2002), whereas inhibitory Nodal cues establish the ectoderm competence of the anterior epiblast (Camus et al., 2006; Perea-Gomez et al., 2002). Nonetheless, *in vitro*, epiblast-like cells (human embryonic stem cell [hESC]- and induced pluripotent stem cell [iPSC]-derived 2D gastruloids) arrange the germ layers in a defined concentric pattern (Warmflash et al., 2014), and 3D gastruloids self-organize along an anteroposterior axis (Moris et al., 2020) in the absence of polarized extraembryonic signals. This evidence highlights the relevance of cell-intrinsic mechanisms regulating the activity of Nodal signaling during gastrulation.

The Hippo pathway regulates organ size, regeneration, and cell growth by controlling the stability of transcription factors YAP1 and TAZ. Hippo/MST kinase cascades phosphorylate YAP1/TAZ, leading to their degradation. When the Hippo kinases are inactive, YAP1/TAZ translocate into the nucleus, where they associate with TEA domain family member 1–4 DNA-binding proteins and regulate transcription (Zhao et al., 2008). YAP1 knockout (KO) embryos die soon after gastrulation (Morin-Kensicki et al., 2006), and a recent

study revealed that YAP1 signaling may act as a molecular determinant in the epiblast (Peng et al., 2019). Furthermore, we and others have previously reported that YAP1 represses mesoendodermal (ME) differentiation in hESCs by regulating the activity of the Nodal and WNT3 pathways (Beyer et al., 2013; Estarás et al., 2017; Hsu et al., 2018). This evidence suggests an important role of YAP1 in gastrulation; however, functional studies are needed to establish the role of YAP1 in this developmental process.

Here, we used a robust model of human gastrulation (Martyn et al., 2018; Warmflash et al., 2014) to examine YAP1-dependent regulatory mechanisms. Our findings indicate that YAP1 KO-derived gastruloids display cell-fate patterning defects associated with an increased dosage of Nodal signaling, incompatible with ectoderm differentiation. Accordingly, inhibiting Nodal signaling can partially rescue the gastrulation defects of YAP1 KO hESCs. Overall, our findings reveal an essential role of YAP1 controlling gastrulation patterning in hESCs.

RESULTS

YAP1 is required for cell-fate patterning of hESC-derived 2D gastruloids

To examine the role of YAP1 in human gastrulation, we analyzed the differentiation pattern of the three germinal layers in 2D-micropatterned gastruloids derived from hESCs (Warmflash et al., 2014). Micropatterned colonies were treated with bone morphogenetic protein 4 (BMP4) cytokine to differentiate them into self-organized concentric rings of embryonic germ layers: ectoderm in the center,
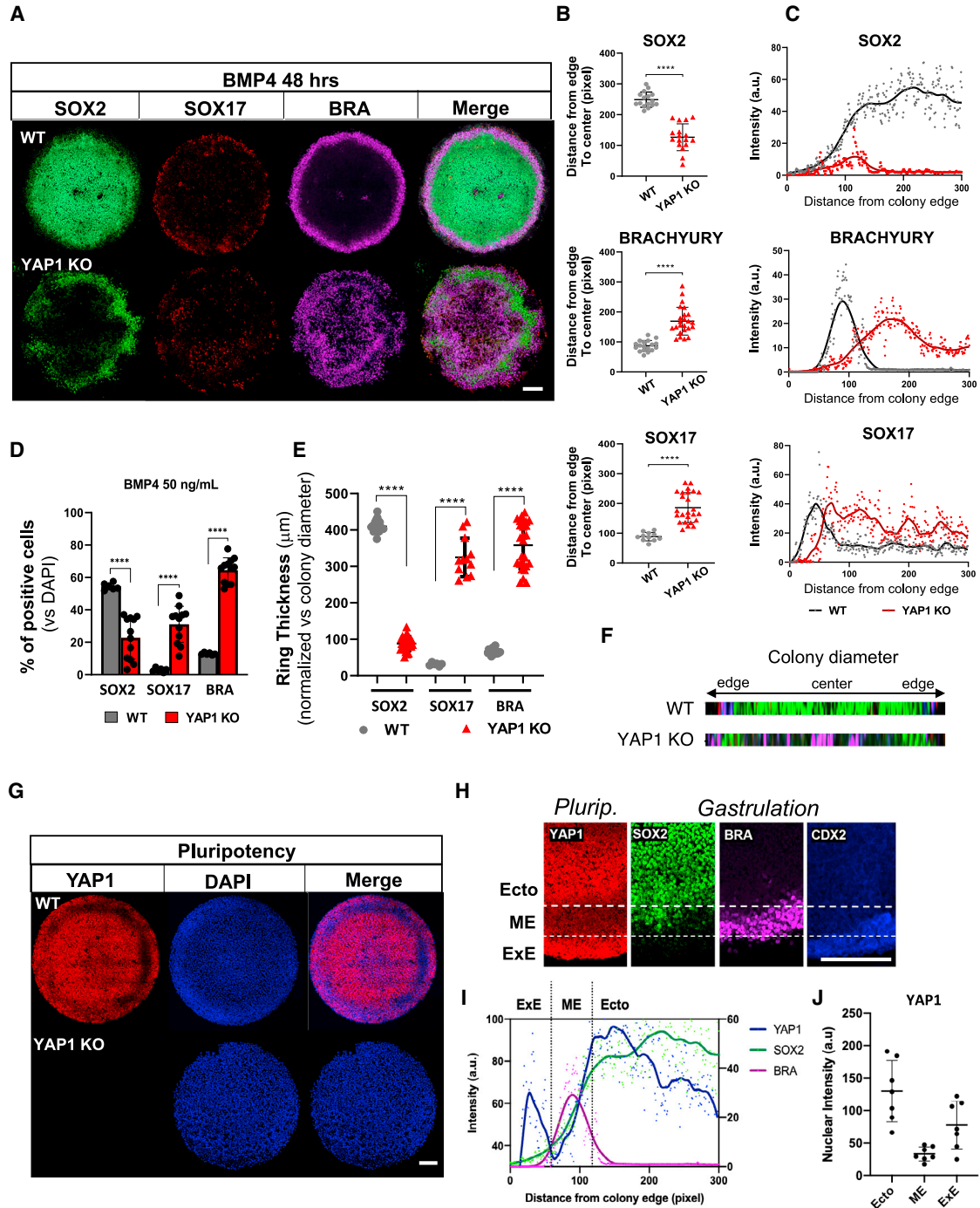
Figure 1. YAP1 regulates the formation of the three germinal layers in hESC-derived 2D gastruloids

(A) Representative immunostaining for the germinal layer markers SOX2 (ectoderm), SOX17 (endoderm), and BRACHYURY/T (BRA, mesoderm) in WT and YAP1 KO micropatterned cell cultures stimulated with BMP4 for 48 h.

(B) Graphs show the position of the maximal intensity peak for the indicated markers across the ratio of the 2D gastruloids. On the y axis, 0 pixels is the edge and 300 pixels is the middle of the colony.

(C) Average fluorescence intensity of indicated markers from edge to colony center.

(D) Percentage of cells positive for analyzed markers versus the total number of cells in the pattern (DAPI).

(E) Quantification of ring thickness of germinal layers in the indicated 2D gastruloids.

(legend continued on next page)

extraembryonic tissue at the edge, and mesoderm and endoderm in between (Warmflash et al., 2014) (Figures 1A–1F and S1A, wild-type [WT] hESCs). We compared the patterned structures derived from WT and YAP1 KO hESCs and found that the number of ectoderm-positive cells expressing the SOX2 and OTX2 markers (Deglincerti et al., 2016) was significantly reduced in the YAP1 KO gastruloids compared with WT. Consequently, the ectodermal layer in the YAP1 KO gastruloids was reduced and became restricted to a ring in the middle-outer part of the colony (Figures 1A–1E and S1A–S1D). However, the percentage of cells positive for mesoderm (BRACHYURY/T[+]) and endoderm (SOX17^{+}) markers was higher in the YAP1-deleted micropatterns. Hence, YAP1 KO gastruloids displayed expanded mesoderm and endoderm rings that populated the center of the colony (Figures 1A–1E). Concordantly, YAP1 KO gastruloids retained higher levels of OCT4 compared with WT, which is necessary to specify ME lineages (Thomson et al., 2011; Wang et al., 2012) (Figures S1E and S1F). We also observed a similar gastrulation phenotype in YAP1 KO iPSCs (Figures S1G and S1H). Furthermore, we analyzed the distribution of YAP1 by immunostaining in undifferentiated hESC colonies. We found that the expression of YAP1 is organized in concentric rings in the confluent colony before gastrulation (Figures 1G–1J and S1I). In the periphery of the colony, where the extraembryonic tissue forms (Deglincerti et al., 2016), YAP1 was highly expressed and predominantly nuclear (Figures 1H–1J and S1J, indicated as ExE, CDX2^{+} ring). Near the edge, coinciding with the prospective endoderm and mesoderm rings, YAP1 levels decrease and accumulate in the cytoplasm. In the interior of the colony, we identified a second peak of YAP1 levels, mostly nuclear, that overlapped with the future ectoderm area (Figures 1G–1J, indicated as Ecto), suggesting that the nuclear location of YAP1 is necessary for ectoderm differentiation. Overall, we conclude that YAP1 regulates the fate and allocation of the three germinal layers in hESC-derived 2D gastruloids.

YAP1 KO hESCs fail to differentiate into ectoderm

The analysis of the 2D gastruloids suggests that the acquisition of an ectodermal cell fate is compromised in the YAP1-depleted cells. To study whether YAP1 is necessary for ectoderm induction, we applied directed differentiation approaches in the hESCs. For this, we treated WT and YAP1 KO hESCs with an established ectoderm differentiation medium containing transforming growth factor β (TGF-β)/Nodal and BMP inhibitors (Chambers et al., 2009) for 5 days. The qPCR analysis of PAX6 and NANOG genes suggested that ectoderm differentiation is compromised in the mutant cells (Figure S2A). To examine this further, we applied an unbiased directed differentiation protocol (STEMCELL Technologies No. 05230) to induce differentiation toward ectoderm, mesoderm, and endoderm lineages in WT and YAP1 KO hESCs (Figure 2A). After culturing the cells for 5 days (mesoderm and endoderm) or 7 days (ectoderm) with the lineage-specific medium, we used RNA sequencing (RNA-seq), immunostaining, and western blotting (WB) approaches to examine the expression of the lineage markers in the differentiated cells. The heatmap in Figure 2B shows that as expected, WT cells expressed typical germ-layer markers after the induction of the three lineages. However, following ectoderm induction, the YAP1 KO cells failed to express ectoderm lineage genes, including SOX1, PAX6, and OTX2. Instead, the expression levels of pluripotency markers, such as POU5F1 and NANOG, remained similar to pluripotent conditions (Figure 2B, 2D, 2F, and S2B). A principal-component analysis (PCA) of the RNA-seq datasets confirmed that the ectoderm-induced YAP1 KO hESCs are highly similar to pluripotent cells (Figure 2C). Consistent with previous reports (Beyer et al., 2013; Estarás et al., 2015, 2017; Hsu et al., 2018), the induction of endoderm genes was enhanced in the YAP1 KO cells compared with WT after treatment with endoderm medium (Figures 2B–2E and S2B). Altogether, these findings show that YAP1 specifies ectoderm in hESCs.

YAP1 represses Nodal pathway genes during ectoderm differentiation

We hypothesized that YAP1 KO hESCs carry hyperactive TGF-β/Nodal:SMAD2/3 activity that counteracts ectoderm induction. To test this idea, we applied a signaling pathway analysis to the RNA-seq datasets derived from the WT and

(F) Representative cross-sectional image showing a profile of the radial distribution of the germ-layer markers.

(G) YAP1 immunostaining (Cell Signaling Technology No. 14074) in WT and YAP1 KO hESC micropatterned cell culture in pluripotency.

(H) Magnifications of YAP1 staining on the edge of a micropatterned pluripotent colony (Plurip.), and CDX2, SOX2, and BRACHYURY staining after BMP4 treatment (Gastrulation). Dotted lines delimit rings corresponding to extraembryonic ectoderm (ExE), mesoendoderm (ME), and ectoderm (Ecto) layers.

(I) Average intensity from edge to colony center of YAP1 immunostaining signal in pluripotency. For comparison, SOX2 and BRACHYURY markers are re-plotted from (C), on the right y axis.

(J) Quantification of YAP1 nuclear signal in the three indicated rings in the pluripotent WT hESC colony. Scale bar, 100 μm.

In (B)–(E), graphs show quantification of 20–25 micropatterns from three independent experiments. In (I)–(J), graphs show quantification of 7–10 micropatterns from two independent experiments. In (B), (D), (E), and (J), data show mean ± SD. ****p ≤ 0.001 (Student's t test). See also Figure S1.
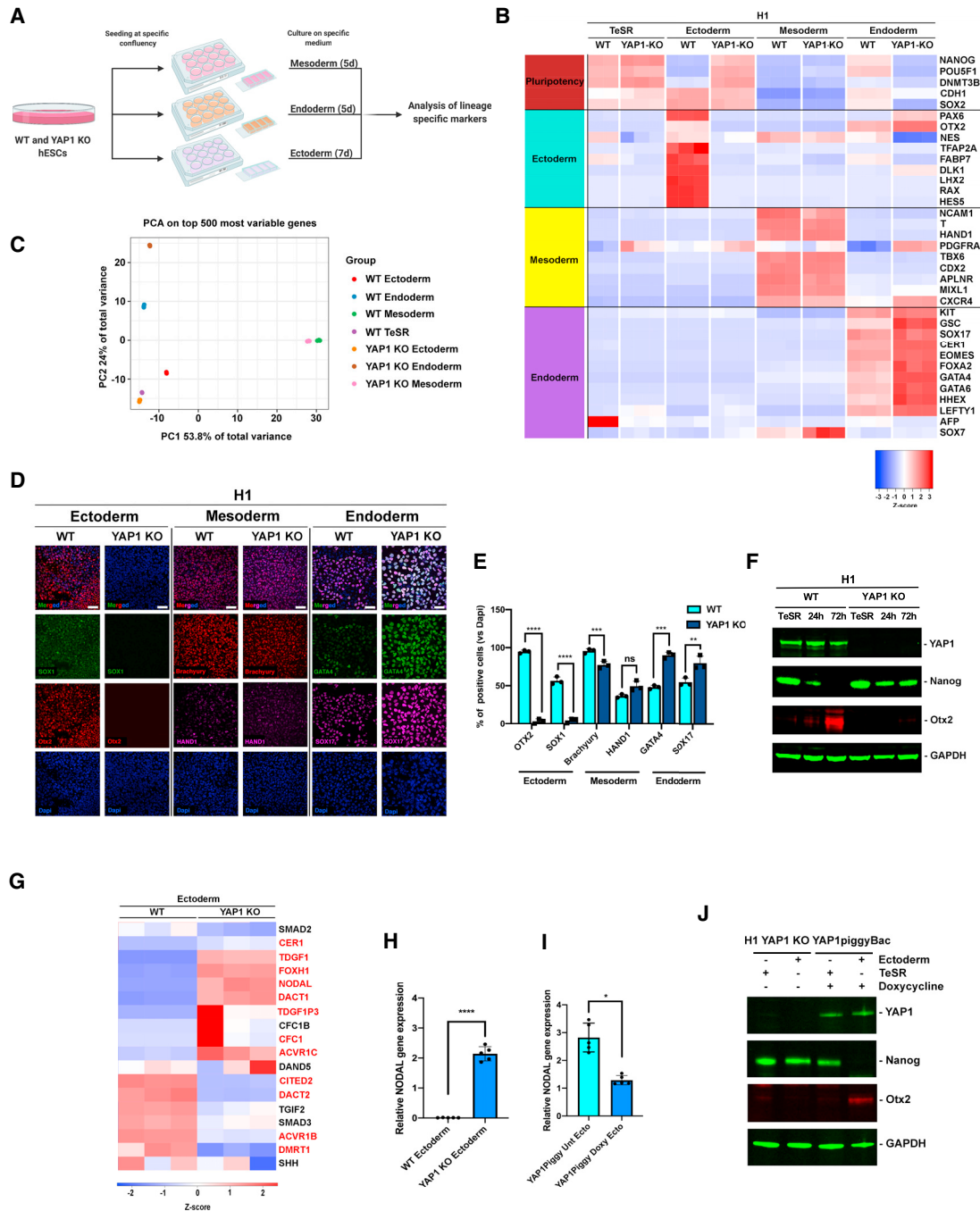
Figure 2. YAP1 is essential for ectoderm fate commitment in directed differentiation

(A) Schematic diagram of the directed differentiation methodology.

(B) Heatmap from RNA-seq analysis showing expression levels of indicated genes after directed differentiation conditions indicated above the map. (Z-scaled log$_2$ fragments per kilobase of transcript per million mapped reads). Three independent replicates are shown for all conditions except for WT hESCs growing in TeSR (n = 2).

(C) Principal-component analysis (PCA) was performed on the 500 most variable genes in WT and YAP1 KO in pluripotency and after directed differentiation.

(D) Immunostaining of WT and YAP1 KO cells after directed differentiation. The cells are stained against specific lineage markers: ectoderm is SOX1 (green) and OTX2 (red); mesoderm is BRACHYURY/T (red) and HAND1 (purple); and endoderm is GATA4 (green) and SOX17 (purple). Nuclei are stained with DAPI. Scale bar, 50 μm.

(legend continued on next page)

YAP1 KO cells after ectoderm induction. We identified 12 genes in the Nodal pathway differentially regulated (DR) in the YAP1 KO cells compared with WT (Figures 2G and S2C). This included the gene that codifies for the transcription factor FOXH1 (log$_2$ fold change [FC] 4.69; adjusted $P <$ .001), an essential nuclear partner of SMAD2/3 in gastrulation (Yamamoto et al., 2001). We also identified upstream components of the Nodal pathway, such as the Activin A receptor ACVR1C (log2 FC 1.92; adjusted $P <$ .001) and the NODAL gene (log2 FC 13.42; adjusted p < 0.001) (Figures 2G, 2H, and S2A). NODAL codifies for the extracellular ligand that activates intracellular SMAD2/3 (Reissmann et al., 2001). Furthermore, we re-introduced YAP1 expression in the YAP1 KO cells using a doxycycline-inducible PiggyBac system (Estarás et al., 2017). We found that re-expressing YAP1 was sufficient to reduce the levels of *NODAL* and recover *OTX2* expression in ectoderm-induced YAP1 KO hESCs (Figure 2I, 2J, and S2D). These results suggest that YAP1 repression of Nodal signaling genes is necessary for ectodermal differentiation.

YAP1 regulates the chromatin accessibility of *FOXH1* and *NODAL* developmental genes

To understand the transcriptional regulatory mechanisms of YAP1 that regulate the exit of pluripotency in hESCs, we applied cutting-edge single-nucleus assay for transposase-accessible chromatin using sequencing (snATAC-seq) technology to examine the genome-wide chromatin accessibility profile in WT and YAP1 KO hESCs. We identified 10,683 DR regions in the YAP1 KO cells compared with WT (representing 3.4% of total peaks). Among them, 8,221 and 2,462 regions lost and gained accessibility in the YAP1 KO cells versus WT, respectively (log$_2$ FC > 1; adjusted p < 0.05) (Figures 3A and 3B). As expected, the DNA motif most represented in regions that lost accessibility in the absence of YAP1 was TEAD4, followed by SOX15 and JUN-AP-1 motifs. Convergently, the DNA motifs recognized by BORIS, ERG, and FOXH1 transcription factors gained access in the YAP1 KO cells (Figure 3C). Importantly, we identified proximal regions near *NODAL* (log$_2$ FC 0.66; adjusted p = 0.052) and *FOXH1* (log$_2$ FC 0.87; adjusted p = .04) genes

that gained accessibility in the YAP1 KO hESCs compared with WT (Figure 3D), which correlated with significantly lower levels of total histone H3 on the regulatory regions of these genes (Figure S3A). Furthermore, our chromatin immunoprecipitation sequencing (ChIP-seq) analysis of YAP1 protein in WT and YAP1 KO hESCs (Estarás et al., 2017) revealed a bona fide YAP1-binding site in the proximal epiblast enhancer (PEE) of *NODAL* (Robertson, 2014; Vincent et al., 2003) and an enhancer ∼8.5 kb upstream of the *FOXH1* transcription start site (TSS) (Figures 3E and S3B). Altogether, these data show that YAP1 directly represses key developmental enhancers on *NODAL* and *FOXH1* genes during ectoderm induction in hESCs.

Cytoplasmic retention of SMAD2/3 during ectoderm induction depends on YAP1

We reasoned that the increased expression of Nodal signaling genes in YAP1 KO cells will lead to the nuclear retention of SMAD2/3 during ectoderm induction. Indeed, we detected an increase in SMAD2/3 levels and a greater accumulation of nuclear SMAD2/3 in response to ectoderm induction in the YAP1 KO cells compared with WT (Figures 3F, 3G, S3C, and S3D). However, we did not detect differences in the subcellular location of SMAD1.5 between WT and YAP1 KO cells (Figures S3C and S3D). Furthermore, we examined SMAD2/3 activity in a 2D neurulation model (Haremaki et al., 2019). In the WT neuruloids, SMAD2/3 was vastly cytoplasmic, and the incipient formation of neural rosettes was observed by the accumulation of SOX2$^+$ cells in the interior part of the colony (Haremaki et al., 2019). In the YAP1 KO, the SMAD2/3 remained predominantly nuclear, consistent with a broader and lower expression of SOX2$^+$ cells across the colony (Figures 3H–3J and S3E). Overall, these findings show that YAP1 KO cells retain higher levels of active SMAD2/3, incompatible with neuroectodermal differentiation (Figure 3K).

Partial inhibition of the nodal pathway rescues the phenotype of YAP1 KO gastruloids

To investigate whether the persistent activity of Nodal: SMAD2/3 signaling underlies the defective differentiation

(E) Quantification of percentage of positive cells for the indicated markers. Nuclei are stained with DAPI. Data show mean ± SD from three independent experiments.

(F) Representative immunoblot of the indicated proteins in WT and YAP1 KO cells growing in TeSR or ectoderm medium for 24 and 72 h. GAPDH was used as a loading control. The experiment was repeated three times with consistent results.

(G) Heatmap from RNA-seq depicts Nodal pathway regulatory genes in WT and YAP1 KO hESCs differentiated to ectoderm. Differentially regulated genes are highlighted in red (p < 0.001, Fisher exact test).

(H and I) Graphs show qPCR analysis of NODAL mRNA levels in WT and YAP1 KO cells (H) or YAP1 KO:YAP1-PiggyBac cells in the presence or absence of doxycycline (I). Data show mean ± SD from five independent experiments.

(J) Representative immunoblot of indicated proteins in YAP1 KO:YAP1-PiggyBac cells treated as indicated above the panel. The experiment was repeated two times with consistent results.

***p < 0.001 (Student's t test). See also Figure S2.
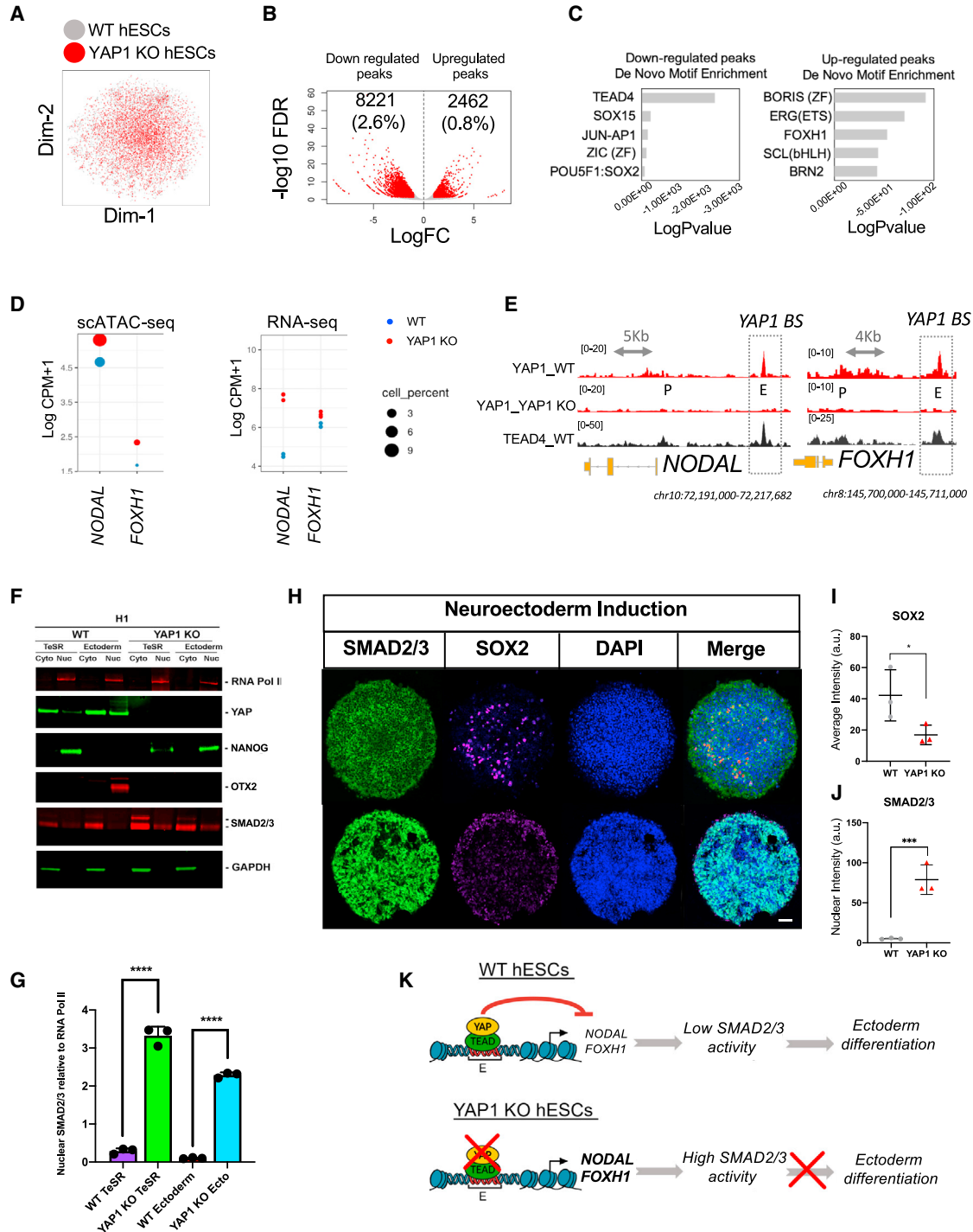
Figure 3. YAP1 inhibits Nodal:SMAD2/3 signaling during ectodermal differentiation

(A) Analysis of snATAC-seq experiments in WT and YAP1 KO hESCs. t-Distributed stochastic neighbor embedding (t-SNE) showing unbiased clustering results for all sequenced cells.

(B) Volcano plot shows differentially regulated (DR) regions in YAP1 KO hESCs versus WT (false discovery rate < 0.05; $\log_2$ FC > 1). Dots are colored by significance (red, significant; gray, not significant).

(C) scATAC-seq analysis of DNA motifs differentially enriched in YAP1 KO versus WT hESCs. The p value for each motif is shown on the x axis of the graph.

(legend continued on next page)

phenotypes of YAP1 KO hESCs, we examined the effect of blocking Nodal signaling in the YAP1 KO gastruloids. We replicated the 2D gastrulation experiments in the YAP1 KO cells in the presence and absence of the Nodal receptor inhibitor A83-0159 (Tojo et al., 2005). Figure 4 shows that co-treatment of BMP4 and the Nodal inhibitor rescued the expression and patterning of the ectoderm layer (SOX2^{+}) in the YAP1 KO 2D gastruloids compared with BMP4 treatment alone (Figures 4A–4D). Accordingly, an outer layer of BRACHYURY/T^{+} cells is visualized around the SOX2^{+} cells in the YAP1 KO gastruloids exposed to BMP4+A83-0159, partially resembling the original structure of WT gastruloids (Figures 4A–4D). We noticed that longer exposures to A83-0159 (48 h) entirely blocked the activity of SMADs and even compromised the formation of the mesoderm and endoderm layers (Figures S4A and S4B). Accordingly, increasing the amount of Nodal inhibitor was sufficient to rescue the YAP1 KO phenotypes in directed differentiation experiments (Figures S4C–S4E). Altogether, these findings show that YAP1 regulates Nodal signaling to coordinate cell fate decisions during human gastrulation.

DISCUSSION

We interrogated the role of YAP1 in the process of gastrulation in hESCs. Our studies revealed three main findings: (1) YAP1 regulates the correct specification and allocation of the three germinal layers in 2D gastruloids, (2) YAP1 is needed to induce an ectodermal fate in hESCs, and (3) YAP1 has a predominant role in repressing the activity of Nodal signaling.

Our findings show that the subcellular distribution of YAP1 is regulated across the pluripotent colony. We speculate that the observed cytoplasmic retention of YAP1 in the ME layer may be crucial to allow Nodal:SMAD2/3 signaling and specify the mesoderm and endoderm layers. In contrast, the internal ring of nuclear YAP1 may act as a barrier to restrict Nodal:SMAD2/3 signaling to allow ectodermal differentiation. This model fits with our previously published data

(Estarás et al., 2017; Hsu et al., 2018) and the observed expansion of the mesoderm and endoderm layers in the YAP1 KO gastruloids. However, the factors that determine YAP1 concentric expression require further investigation. Previous studies have shown that key signaling components involved in gastrulation also display spatial ordering in the pluripotent colony, including SMAD2/3 and β-catenin (Martyn et al., 2019; Warmflash et al., 2014). The distribution of these factors is controlled by cell density, E-cadherin levels or the state of E-cadherin junctions in the periphery of the colony compared with the center, or spatial restriction of upstream signaling components in defined rings (Etoc et al., 2016; Martyn et al., 2019; Warmflash et al., 2014). Interestingly, E-cadherin may act as an upstream cell-surface receptor that regulates Hippo signaling kinases in response to cell-cell contact (Kim et al., 2011). Thus, we speculate that the reduction of nuclear YAP1 in the prospective ME layer may be caused by cell-cell contact-mediated activation of the Hippo kinases.

Overall, our findings suggest that YAP1 regulates BMP4-induced gastrulation by restricting Nodal signaling. However, overly active Nodal signaling may not explain the unexpected location of the ectodermal ring in the outer part of the colony in the YAP1 KO gastruloids. In fact, a recent report (bioRxiv, not yet peer reviewed) showed that an increased Activin/Nodal:SMAD2/3 signal caused by mutations in the Huntingtin gene results in the expansion of mesoderm and endoderm layers in the 2D gastruloids without affecting the location of the ectoderm layer (Galgoczi et al., 2021). Furthermore, in the 2D gastruloids, co-treatment with BMP4 and a Nodal inhibitor causes a reduction of the mesoderm and endoderm layers and expansion of the ectoderm but does not affect the location of layers (Martyn et al., 2018). Hence, additional work is needed to comprehend the YAP1-regulatory mechanisms that lie beneath the patterning defects of the YAP1 KO gastruloids.

Overall, our findings have established an exciting connection between Nodal and YAP1 pathways in gastrulation,

(D) Dot plot graph from the scATAC-seq analysis displays a regulated peak near the TSS of FOXH1 and NODAL genes (±10 kb). The RNA-seq graph is included for comparison. LogCPM+1, log counts per million.

(E) Genome browser captures of ChIP-seq analysis of indicated proteins in WT and YAP1 KO hESCs (from Estarás et al., 2017). ChIP-seq identified a YAP1-binding site (BS) in the enhancer (E) near *NODAL* and *FOXH1* genes. P, promoter.

(F) Representative immunoblot of indicated proteins in cytoplasmic and nuclear sub-fractions from WT and YAP1 KO cells, treated as indicated.

(G) Quantification of nuclear SMAD2/3 bands in WB in (F). Data show mean ± SD from three independent experiments. ****$p < 0.0001$ (Student's t test).

(H) Immunostaining of indicated markers in WT and YAP1 KO-derived neuruloids after 4 days' treatment in neurulation media.

(I and J) Quantification of average fluorescence intensity of SOX2 (I) and nuclear intensity of SMAD2/3 (J) in WT and YAP1 KO structures. Scale bar, 50 μm. Three micropatterns were quantified from one experiment (mean ± SD). *$p < 0.05$ and ***$p < 0.001$ (Student's t test).

(K) Scheme of YAP1 role in ectoderm induction.

See also Figure S3.
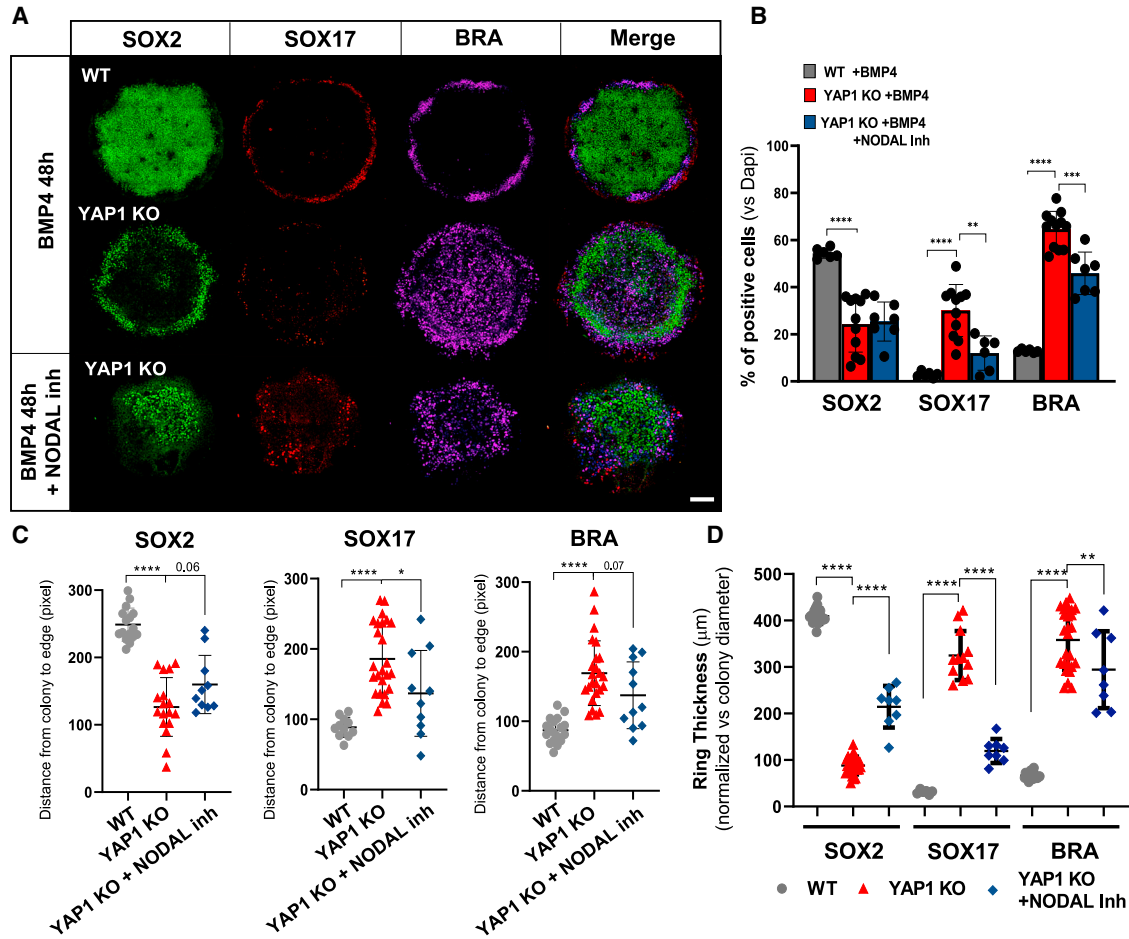
Figure 4. Nodal inhibition rescues 2D gastrulation defects in YAP1 KO cells

(A) Immunostaining for indicated germinal layer markers in YAP1 KO micropatterned cell cultures stimulated with BMP4 (50 ng/mL) or combined BMP4 +Nodal inhibitor (A83-0159 1 μM). WT 2D gastruloids are shown for comparison.

(B) Percentage of SOX2^{+}, SOX17^{+}, and BRACHYURY/T[+] (BRA) cells in WT and YAP1 KO gastruloids in the presence or absence of Nodal inhibitor.

(C and D) Position of maximal intensity peak from the colony edge (C) and ring thickness (D) for the three germinal layer markers in the indicated gastruloids. In (C), 0 pixels on the y axis is the edge of the colony. Scale bar, 100 μm. A total of 20–25 micropatterns were quantified from two independent experiments (mean ± SD; **p < 0.01 and ****p < 0.001, unpaired t test).

See also Figure S4.

---

opening the door to future studies on investigating the Nodal:YAP1 regulatory axis *in vivo*.

EXPERIMENTAL PROCEDURES

Detailed methods are provided in the Supplemental experimental procedures. Table S1 contains the list of antibodies and primers used in this study.

hESC culture and cell lines

hESC and iPSC (human pluripotent stem cell [hPSC]) lines were cultured in mTeSR1 medium on Matrigel-coated tissue culture plates. WT, YAP1 KO, and the doxycycline-inducible YAP1 (YAP1 KO:FLA-GYAP1-PiggyBac) H1 hESCs were previously described elsewhere.[13]

CRISPR-Cas9 was applied to generate a new YAP1 KO cell line from parental EC11 iPSCs following the same method described in Estarás et al., 2017).

Micropattern cell culture and gastrulation induction

To generate 2D gastruloids, hPSCs were seeded on micropatterned glass chips from CYTOO (CYTOOchips Arena 1000, Grenoble, France) and treated with BMP4 50 ng/mL for 48 h, following described procedures (Deglincerti et al., 2016). For the analysis of pluripotent colonies, cells were fixed when they reached 90% confluency, before BMP4 treatment.

Accession numbers

Full datasets of single-cell assay for transposase-accessible chromatin using sequencing (scATAC-seq) and RNA-seq can be accessed via

GEO: GSE168377. The ChIP-seq datasets can be accessed in GEO: GSE99202.

AUTHOR CONTRIBUTIONS

C.E. and H.H. conceived the project and performed initial experiments. C.E. supervised micropattern experiments, designed the experiments, wrote the manuscript, and attained funding. K.A.J. supervised directed differentiation experiments and attained funding. S.G. designed and performed directed differentiation experiments and analysis and prepared figures. E.S. designed and performed experiments in the micropatterns and their corresponding analysis and prepared figures. E.A. assisted with the micropattern experiments, quantification of figures, and analysis of the PEE. G.R.M. and E.A. developed the MATLAB core. L.H. performed all bioinformatics analysis of the sequencing data and generated the corresponding figures. S.G., E.S., H.H., E.A., and L.H. reviewed and edited the manuscript.

CONFLICTS OF INTEREST

The authors declare no competing interests.

REFERENCES

Arnold, S.J., and Robertson, E.J. (2009). Making a commitment: cell lineage allocation and axis patterning in the early mouse embryo. Nat. Rev. Mol. Cell Biol. *10*, 91–103. https://doi.org/10.1038/nrm2618.

Beyer, T.A., Weiss, A., Khomchuk, Y., Huang, K., Ogunjimi, A.A., Varelas, X., and Wrana, J.L. (2013). Switch enhancers interpret TGF-β and Hippo signaling to control cell fate in human embryonic stem cells. Cell Rep. *5*, 1611–1624. https://doi.org/10.1016/j.celrep.2013.11.021.

Brennan, J., Lu, C.C., Norris, D.P., Rodriguez, T.A., Beddington, R.S., and Robertson, E.J. (2001). Nodal signalling in the epiblast patterns the early mouse embryo. Nature *411*, 965–969. https://doi.org/10.1038/35082103.

Brennan, J., Norris, D.P., and Robertson, E.J. (2002). Nodal activity in the node governs left-right asymmetry. Genes Dev. *16*, 2339–2344. https://doi.org/10.1101/gad.1016202.

Camus, A., Perea-Gomez, A., Moreau, A., and Collignon, J. (2006). Absence of Nodal signaling promotes precocious neural differentiation in the mouse embryo. Dev. Biol. *295*, 743–755. https://doi.org/10.1016/j.ydbio.2006.03.047.

Chambers, S.M., Fasano, C.A., Papapetrou, E.P., Tomishima, M., Sadelain, M., and Studer, L. (2009). Highly efficient neural conversion of human ES and iPS cells by dual inhibition of SMAD signaling. Nat. Biotechnol. *27*, 275–280. https://doi.org/10.1038/nbt.1529.

Deglincerti, A., Etoc, F., Guerra, M.C., Martyn, I., Metzger, J., Ruzo, A., Simunovic, M., Yoney, A., Brivanlou, A.H., Siggia, E., and Warmflash, A. (2016). Self-organization of human embryonic stem cells on micropatterns. Nat. Protoc. *11*, 2223–2232. https://doi.org/10.1038/nprot.2016.131.

Estarás, C., Benner, C., and Jones, K.A. (2015). SMADs and YAP compete to control elongation of β-catenin:LEF-1-recruited RNAPII during hESC differentiation. Mol. Cell *58*, 780–793. https://doi.org/10.1016/j.molcel.2015.04.001.

Estarás, C., Hsu, H.T., Huang, L., and Jones, K.A. (2017). YAP repression of the Wnt3 gene controls hESC differentiation along the cardiac mesoderm lineage. Genes Dev. *31*, 2250–2263. https://doi.org/10.1101/gad.307512.117.

Etoc, F., Metzger, J., Ruzo, A., Kirst, C., Yoney, A., Ozair, M.Z., Brivanlou, A.H., and Siggia, E.D. (2016). A Balance between secreted inhibitors and edge Sensing controls gastruloid self-organization. Dev. Cell *39*, 302–315. https://doi.org/10.1016/j.devcel.2016.09.016.

Galgoczi, S., Albert, R., Markopoulos, C., Anna, Y., Phan-Everson, T., Haremaki, T., Metzger, J.J., Etoc, F., and Brivanlou, A.H. (2021). Huntingtin CAG expansion impairs germ layer patterning in synthetic human gastruloids through polarity defects. Development *148*, dev199513.

Haremaki, T., Metzger, J.J., Rito, T., Ozair, M.Z., Etoc, F., and Brivanlou, A.H. (2019). Self-organizing neuruloids model developmental aspects of Huntington's disease in the ectodermal compartment. Nat. Biotechnol. *37*, 1198–1208. https://doi.org/10.1038/s41587-019-0237-5.

Hsu, H.T., Estarás, C., Huang, L., and Jones, K.A. (2018). Specifying the anterior primitive streak by modulating YAP1 levels in human pluripotent stem cells. Stem Cell Rep. *11*, 1357–1364. https://doi.org/10.1016/j.stemcr.2018.10.013.

Kim, N.G., Koh, E., Chen, X., and Gumbiner, B.M. (2011). E-cadherin mediates contact inhibition of proliferation through Hippo signaling-pathway components. Proc. Natl. Acad. Sci. U S A *108*, 11930–11935. https://doi.org/10.1073/pnas.1103345108.

Martyn, I., Kanno, T.Y., Ruzo, A., Siggia, E.D., and Brivanlou, A.H. (2018). Self-organization of a human organizer by combined Wnt and Nodal signalling. Nature *558*, 132–135. https://doi.org/10.1038/s41586-018-0150-y.

Martyn, I., Brivanlou, A.H., and Siggia, E.D. (2019). A wave of WNT signaling balanced by secreted inhibitors controls primitive streak

formation in micropattern colonies of human embryonic stem cells. Development *146*. https://doi.org/10.1242/dev.172791.

Meno, C., Gritsman, K., Ohishi, S., Ohfuji, Y., Heckscher, E., Mochida, K., Shimono, A., Kondoh, H., Talbot, W.S., Robertson, E.J., et al. (1999). Mouse Lefty2 and zebrafish antivin are feedback inhibitors of nodal signaling during vertebrate gastrulation. Mol. Cell *4*, 287–298. https://doi.org/10.1016/s1097-2765(00)80331-7.

Morin-Kensicki, E.M., Boone, B.N., Howell, M., Stonebraker, J.R., Teed, J., Alb, J.G., Magnuson, T.R., O'Neal, W., and Milgram, S.L. (2006). Defects in yolk sac vasculogenesis, chorioallantoic fusion, and embryonic axis elongation in mice with targeted disruption of Yap65. Mol. Cell Biol. *26*, 77–87. https://doi.org/10.1128/MCB.26.1.77-87.2006.

Moris, N., Anlas, K., van den Brink, S.C., Alemany, A., Schröder, J., Ghimire, S., Balayo, T., van Oudenaarden, A., and Martinez Arias, A. (2020). An in vitro model of early anteroposterior organization during human development. Nature *582*, 410–415. https://doi.org/10.1038/s41586-020-2383-9.

Peng, G., Suo, S., Cui, G., Yu, F., Wang, R., Chen, J., Chen, S., Liu, Z., Chen, G., Qian, Y., et al. (2019). Molecular architecture of lineage allocation and tissue organization in early mouse embryo. Nature *572*, 528–532. https://doi.org/10.1038/s41586-019-1469-8.

Perea-Gomez, A., Vella, F.D., Shawlot, W., Oulad-Abdelghani, M., Chazaud, C., Meno, C., Pfister, V., Chen, L., Robertson, E., Hamada, H., et al. (2002). Nodal antagonists in the anterior visceral endoderm prevent the formation of multiple primitive streaks. Dev. Cell *3*, 745–756. https://doi.org/10.1016/s1534-5807(02)00321-0.

Reissmann, E., Jörnvall, H., Blokzijl, A., Andersson, O., Chang, C., Minchiotti, G., Persico, M.G., Ibáñez, C.F., and Brivanlou, A.H. (2001). The orphan receptor ALK7 and the Activin receptor ALK4 mediate signaling by Nodal proteins during vertebrate development. Genes Dev. *15*, 2010–2022. https://doi.org/10.1101/gad.201801.

Robertson, E.J. (2014). Dose-dependent Nodal/Smad signals pattern the early mouse embryo. Semin. Cell Dev. Biol. *32*, 73–79. https://doi.org/10.1016/j.semcdb.2014.03.028.

Thomson, M., Liu, S.J., Zou, L.N., Smith, Z., Meissner, A., and Ramanathan, S. (2011). Pluripotency factors in embryonic stem cells regulate differentiation into germ layers. Cell *145*, 875–889. https://doi.org/10.1016/j.cell.2011.05.017.

Tojo, M., Hamashima, Y., Hanyu, A., Kajimoto, T., Saitoh, M., Miyazono, K., Node, M., and Imamura, T. (2005). The ALK-5 inhibitor A-83-01 inhibits Smad signaling and epithelial-to-mesenchymal transition by transforming growth factor-beta. Cancer Sci. *96*, 791–800. https://doi.org/10.1111/j.1349-7006.2005.00103.x.

Vincent, S.D., Dunn, N.R., Hayashi, S., Norris, D.P., and Robertson, E.J. (2003). Cell fate decisions within the mouse organizer are governed by graded Nodal signals. Genes Dev. *17*, 1646–1662. https://doi.org/10.1101/gad.1100503.

Wang, Z., Oron, E., Nelson, B., Razis, S., and Ivanova, N. (2012). Distinct lineage specification roles for NANOG, OCT4, and SOX2 in human embryonic stem cells. Cell Stem Cell *10*, 440–454. https://doi.org/10.1016/j.stem.2012.02.016.

Warmflash, A., Sorre, B., Etoc, F., Siggia, E.D., and Brivanlou, A.H. (2014). A method to recapitulate early embryonic spatial patterning in human embryonic stem cells. Nat. Methods *11*, 847–854. https://doi.org/10.1038/nmeth.3016.

Yamamoto, M., Meno, C., Sakai, Y., Shiratori, H., Mochida, K., Ikawa, Y., Saijoh, Y., and Hamada, H. (2001). The transcription factor FoxH1 (FAST) mediates Nodal signaling during anterior-posterior patterning and node formation in the mouse. Genes Dev. *15*, 1242–1256. https://doi.org/10.1101/gad.883901.

Zhao, B., Ye, X., Yu, J., Li, L., Li, W., Li, S., Lin, J.D., Wang, C.Y., Chinnaiyan, A.M., Lai, Z.C., and Guan, K.L. (2008). TEAD mediates YAP-dependent gene induction and growth control. Genes Dev. *22*, 1962–1971. https://doi.org/10.1101/gad.1664408.